

# Comparison and analysis of two aerosol retrievals over the ocean in the Terra/Clouds and the Earth's Radiant Energy System–Moderate Resolution Imaging Spectroradiometer single scanner footprint data: 1. Global evaluation

Tom X.-P. Zhao,<sup>1,2</sup> Istvan Laszlo,<sup>2</sup> Patrick Minnis,<sup>3</sup> and Lorraine Remer<sup>4</sup>

Received 8 February 2005; revised 20 June 2005; accepted 23 August 2005; published 9 November 2005.

[1] Satellite aerosol remote sensing entered a new era with the deployment of advanced satellite imaging instruments such as the Moderate Resolution Imaging Spectroradiometer (MODIS) on the NASA Terra and Aqua satellites. These new instruments provide the opportunity to learn more about aerosol properties than was possible using the simpler NOAA Advanced Very High Resolution Radiometer (AVHRR), which has been used to retrieve aerosol optical thickness for more than 20 years. Combining historical AVHRR and the more advanced MODIS aerosol retrievals to form a long-term aerosol data record is critical for studying aerosol climate forcing. To achieve this objective, it is necessary to build a connection and establish consistency between the two retrievals through a careful evaluation of the two retrieval methods applied to the same data. As a first step in this effort, this paper exploits the potential of the Clouds and the Earth's Radiant Energy System (CERES) Single-Scanner Footprint (SSF) data set that includes aerosol products derived from Terra MODIS data at the same locations using both the multichannel MODIS and the two-channel AVHRR aerosol retrieval algorithms. The analysis examines the differences in the results seen over oceans on a global scale. It was found in a global mean sense that advancement in the aerosol retrieval over ocean from the MODIS algorithm relative to the AVHRR method is realized mostly in the improvement of the aerosol size parameter (ASP) rather than in the aerosol optical thickness (AOT). However, regional differences were observed in both AOT and ASP retrieved from the MODIS and AVHRR algorithms. These are examined further in the second part of this two-part paper. Cloud contamination and surface roughness appear to affect both aerosol retrievals, effects that need further investigation.

**Citation:** Zhao, T. X.-P., I. Laszlo, P. Minnis, and L. Remer (2005), Comparison and analysis of two aerosol retrievals over the ocean in the Terra/Clouds and the Earth's Radiant Energy System–Moderate Resolution Imaging Spectroradiometer single scanner footprint data: 1. Global evaluation, *J. Geophys. Res.*, *110*, D21208, doi:10.1029/2005JD005851.

## 1. Introduction

[2] It is widely recognized that aerosols cause the largest uncertainties in assessing the radiative forcing of climate by atmospheric constituents generated by anthropogenic activity [Intergovernmental Panel on Climate Change, 2001]. Nonintrusive satellite observations are a unique tool for monitoring the global distribution of aerosol particles and can be used to reduce those uncertainties [King *et al.*,

1999; Kaufman *et al.*, 2002; Mischenko *et al.*, 2004]. Satellite aerosol remote sensing has entered a new era because of the successful deployment of advanced satellite imaging instruments such as the Moderate Resolution Imaging Spectroradiometer (MODIS) and the Multiangle Imaging Spectroradiometer (MISR) on the NASA Earth Observing System satellites, Terra and Aqua.

[3] Satellite aerosol retrievals require a very careful separation of the relatively weak aerosol signal from the other factors influencing the retrieval including those associated with radiometric and calibration errors of the sensors, inaccurate assumptions in the retrieval algorithm, variable atmospheric gas absorption and surface reflectance, and cloud contamination [Tanré *et al.*, 1996; Mischenko *et al.*, 1999]. These uncertainties, which are associated with all aerosol retrievals from satellite sensors, such as the Advanced Very High Resolution Radiometer (AVHRR), are a major concern in applying historical satellite aerosol data in global aerosol radiative forcing studies [Penner *et al.*,

<sup>1</sup>Earth System Science Interdisciplinary Center, University of Maryland, College Park, Maryland, USA.

<sup>2</sup>Office of Research and Application, NOAA National Environmental Satellite, Data, and Information Service, Camp Springs, Maryland, USA.

<sup>3</sup>Atmospheric Sciences Division, NASA Langley Research Center, Hampton, Virginia, USA.

<sup>4</sup>Laboratory for Atmospheres, NASA Goddard Space Flight Center, Greenbelt, Maryland, USA.

2002]. These uncertainties are expected to be reduced in the aerosol retrievals from more advanced imaging sensors such as MODIS because of its high spectral and spatial resolutions and lower radiometric noise.

[4] Some preliminary comparisons of the more advanced MODIS and simpler AVHRR aerosol retrieval methodologies were recently conducted by *Ignatov et al.* [2005] but they did not systematically evaluate the improvement gained by using the MODIS technique relative to the AVHRR method. Results from the two methodologies applied over the same locations have been combined by the Clouds and the Earth's Radiant Energy (CERES) project in the Terra/CERES-MODIS Single Scanner Footprint (SSF) data [*Wielicki et al.*, 1996, 1997]. The SSF data offer a unique opportunity for such a systematic evaluation. The two retrievals, MODIS [*Remer et al.*, 2005] and AVHRR-type [*Ignatov and Stowe*, 2002], use the radiances from the same source (MODIS) with the same calibration uncertainties. Any differences in their results can be attributed to algorithm issues and sampling approaches but not to instrument radiometric bias.

[5] Intercomparison of these two SSF aerosol products and their validation against surface measurements will help us to quantitatively evaluate the improvement of the MODIS aerosol retrieval as well as to build connection and consistency between the more advanced MODIS aerosol product and the long-term (~20 year) historical AVHRR aerosol record. Moreover, the Terra/CERES-MODIS SSF data include a comprehensive, high-quality compilation of satellite cloud, aerosol, earth radiation budget, and meteorological information (more than 140 parameters). The multiple SSF parameters of cloud and surface properties also offer a unique opportunity for a comprehensive study of cloud and surface roughness effects on both aerosol retrieval techniques.

[6] Detailed comparisons and evaluations of the two SSF aerosol products and the results are summarized in two companion papers. This first paper describes the global (or first-order) comparison and analysis of the two aerosol products in the CERES-MODIS SSF data. The regional (or second-order) comparison and analysis are presented in the second paper. The results contained in these two papers will benefit the studies of aerosol radiative forcing using the SSF data and provide a basis for evaluating the long-term variation in aerosol properties derived from the AVHRR data.

## 2. SSF Data

[7] This study uses the daytime Edition-1A Terra/CERES-MODIS SSF data [*Wielicki et al.*, 1997; *Geier et al.*, 2003] derived for the entire year of 2001. Two sets of SSF data are available in the CERES product and they are derived respectively from the two CERES instruments aboard the Terra satellite platform. The first set is derived from the CERES instrument operating in a cross-track (CT) scan mode, called Flight Mode 1 (FM1). The second set is derived from the CERES instrument operating in biaxial scan mode, called Flight Mode 2 (FM2), to provide new angular flux information. Broadband radiative fluxes from the CERES, CERES-derived cloud data and aerosol parameters from the MODIS measurements, and assimilated

meteorological fields are mapped into a single CERES footprint with a spatial resolution of about  $20 \text{ km} \times 20 \text{ km}$  at nadir. Both sets use the same cloud and aerosol fields derived from the MODIS data.

[8] There are two aerosol products (I and II) in the SSF data set. Product I is obtained by averaging the standard 10-km MODIS aerosol products [see *Kaufman et al.*, 1997; *Tanré et al.*, 1997; *Remer et al.*, 2005] in each CERES footprint weighted by the CERES Point Spread Function (PSF). The MODIS aerosol retrieval over ocean is based on a multichannel algorithm and is sensitive to aerosol type since the solution is determined from 20 possible combinations of aerosol model output (four aerosol models for small particles and five aerosol models for large particles). The retrieval assumes a wind speed of 6 m/s. The standard MODIS cloud mask termed as MOD35 for Terra [*Ackerman et al.*, 1998] and a spatial variability test [*Martins et al.*, 2002] are used to determine clear-sky radiances. A total of 29 output parameters constitute the standard MODIS ocean aerosol product (refer to *Remer et al.* [2005, Table 7]). Only 15 parameters [see *Ignatov et al.*, 2005, Table 2] are mapped into a CERES footprint to form the CERES SSF MODIS aerosol product. Only two aerosol optical thicknesses ( $\tau_1$  and  $\tau_2$  at  $\lambda_1 = 0.66 \mu\text{m}$  and  $\lambda_2 = 1.60 \mu\text{m}$ , respectively) and the derived Ångström wavelength exponent (AWE) parameter ( $\alpha = -\ln[\tau_1/\tau_2]/\ln[\lambda_1/\lambda_2]$ ) are used here to compare with those derived using the AVHRR-type methodology. The MODIS Collection 3 aerosol product (MOD04) is used in the Edition-1A SSF data.

[9] The AVHRR-type product, product II, is derived from the simple independent two-channel NOAA/NESDIS aerosol retrieval algorithm [*Stowe et al.*, 1997; *Ignatov and Stowe*, 2002; *Zhao et al.*, 2003; *Ignatov et al.*, 2005]. The 1-km MODIS radiances (MOD02 L1B Radiance) are sampled to achieve an effective resolution of 2 km and screened for cloud contamination using the CERES cloud mask scheme [*Trepte et al.*, 1999; *Minnis et al.*, 1995, 1999, 2002]. Pixels that are classified as cloud-free undergo further sunglint screening. Similar to the operational AVHRR aerosol retrieval, clear uniformity and adjacency tests [*Stowe et al.*, 1999; *Vemury et al.*, 2001] are also applied in the AVHRR-type retrieval. The radiances for these filtered clear pixels are then averaged into a CERES footprint according to the CERES PSF to form the so called "aerosol reflectance" for a CERES footprint. This "aerosol reflectance" is input to the AVHRR aerosol retrieval algorithm to make the final retrieval for the footprint. The algorithm assumes a wind speed of 1 m/s but a small diffuse flux is added to the lower boundary to mimic the global mean lower boundary condition. Two optical thicknesses,  $\tau_1$  and  $\tau_2$ , at  $\lambda_1 = 0.66 \mu\text{m}$  and  $\lambda_2 = 1.60 \mu\text{m}$  channels are derived and reported for each CERES clear footprint. We also derive a size parameter  $\alpha (= -\ln[\tau_1/\tau_2]/\ln[\lambda_1/\lambda_2])$  in our analysis and comparison. The major concern for this simple algorithm is the use of a fixed aerosol model so that the retrieval may have difficulty in capturing the regional/temporal aerosol variations [*Zhao et al.*, 2004]. However, the simplicity and economy of the algorithm is still valuable for simpler imaging instruments, such as AVHRR, as long as its performance is carefully evaluated [*Zhao et al.*, 2002, 2003, 2004]. Appendix A provides a detailed description of how the two SSF aerosol retrievals are mapped into the CERES footprints.

[10] *Ignatov et al.* [2005, Table 1] compares the major components of the MODIS and AVHRR-type retrieval algorithms. The sampling approach, cloud screenings, surface reflection computation, and aerosol model assumptions are the four potential processes that can produce differences in the two retrievals. Since sampling issues were discussed in detail by *Ignatov et al.* [2005] using the same SSF aerosol data, we will focus the following analyses on the last three components, which need at least one year of data for a relatively complete investigation. *Ignatov et al.* [2005] found that the difference between the two SSF aerosol products introduced by the dissimilar sampling approaches of the two methods can be neglected for those CERES footprints for which both MODIS and AVHRR-type retrievals are available. To minimize the sampling issue, the current analysis uses only those SSF footprints with both types of aerosol retrievals. Moreover, the analyses focus on the monthly mean values of the two SSF aerosol products, which are subject to fewer sampling effects compared to daily and weekly mean values. Since the MODIS clear-sky radiances serve as input for both retrievals, the uncertainties associated with the instrument biases (an important issue needing a separate study) are eliminated. Thus the present study focuses, as much as possible, on the analysis of the uncertainties associated with the algorithms. This is the biggest advantage of using the SSF data in the comparison of the two aerosol retrievals.

[11] The comparison will focus on monthly mean values of the retrieved aerosol optical thickness (AOT),  $\tau_1$  (at  $\lambda_1 = 0.66 \mu\text{m}$  channel) and  $\tau_2$  (at  $\lambda_2 = 1.60 \mu\text{m}$  channel), and the derived aerosol size parameter (ASP), the Ångström wavelength exponent,

$$\alpha = -\ln[\tau_1/\tau_2]/\ln[\lambda_1/\lambda_2]. \quad (1)$$

[12] Sensitivity tests performed by *Mischenko et al.* [1999] indicate that the monthly mean AOTs are relatively insensitive to the size distributions used in the AVHRR aerosol retrieval compared to the retrieved monthly mean effective radii ( $r_{\text{eff}}$ ), which depends significantly on the aerosol size distribution. However,  $\alpha$  is much less sensitive than  $r_{\text{eff}}$  because it depends entirely on the ratio of the spectral optical thickness. *Ignatov and Stowe* [2000] further explained that the retrieved  $\alpha$  tends to be closer to the real  $\alpha$  rather than to the  $\alpha$  defined by the fixed aerosol model in the AVHRR aerosol retrieval because the departure of  $\tau_1$  and  $\tau_2$  from their real values because of the assumption of a fixed aerosol model is coherent in the two retrieval channels. In other words, if  $\tau_1$  is overestimated for a regional retrieval because of the assumption of an inappropriate aerosol model,  $\tau_2$  is also overestimated (rather than underestimated) and vice versa. The relative magnitude of the overestimation (or underestimation) in the two channels is also comparable according to *Ignatov and Stowe* [2000]. The corresponding errors produced in  $\tau_1$  (or the product of  $\omega_1 P_1$ ) and  $\tau_2$  (or the product of  $\omega_2 P_2$ ) tend to be in a multiplicative rather than additive form as a result of the single scattering formula of aerosol particles,  $\tau \propto [\omega_a P_a(\chi)]^{-1}$ , where  $\omega_a$  ( $\omega_1$  and  $\omega_2$ ) is the aerosol single scattering albedo,  $P_a$  ( $P_1$  and  $P_2$ ) is the aerosol phase function and  $\chi$  is the scattering angle. The errors mostly cancel each other when deriving ASP through the ratio,  $\tau_1/\tau_2$ . Thus, as long as  $\tau_1$  and  $\tau_2$  are retrieved with a

sufficient accuracy (by minimizing sensor radiometric errors, cloud contamination, and surface disturbance) for a fixed aerosol model, the derived  $\alpha$  value should not be limited by the usage of the fixed aerosol model and should fall within its natural range of variability [*Higurashi and Nakajima*, 1999; *Mischenko et al.*, 1999; *Ignatov and Stowe*, 2000]. However, the exact values of  $\alpha$  still depend on the aerosol model used in the retrieval and the fixed aerosol model should be as representative as possible of the global mean condition. *Zhao et al.* [2002, 2004] demonstrated that the AVHRR-type algorithm meets this “global” criterion.

[13] To compare the ASPs, values of  $\alpha$  were computed directly from the AOTs ( $\tau_1$  and  $\tau_2$ ) derived from the MODIS and AVHRR-type algorithms,  $\tau(\text{MODIS})$  and  $\tau(\text{AVHRR})$ , respectively. Because the latter is a “global” algorithm, the differences between the SSF MODIS and AVHRR-type  $\alpha$  values will also strongly depend on the differences between the actual regional and seasonally variant aerosol types and the global model used by the AVHRR-type method. Since the MODIS retrieval attempts to account for the actual aerosol type, it is expected that the SSF MODIS  $\alpha$  values,  $\alpha(\text{MODIS})$ , represent a better seasonal and/or regional variation compared to the SSF AVHRR-type  $\alpha$ ,  $\alpha(\text{AVHRR})$ . This expectation will be carefully examined below and also in the regional evaluation in the work by *Zhao et al.* [2005].

[14] Although some results will be presented for all months during 2001, data from January, April, July, and October will be used to check the seasonal variations in detail. Only CERES FM1 data are used in the analyses since the differences between FM1 and FM2 data are small for a monthly value. Furthermore, only data taken over ocean are compared since the AVHRR-type algorithm is used only over water surfaces.

### 3. Global Comparison of the Two SSF Aerosol Products

[15] Figure 1 shows the global distribution of the monthly mean parameters for March 2001 using  $1^\circ \times 1^\circ$  averages of  $\tau_1$ ,  $\tau_2$ , and  $\alpha$  for the SSF aerosol products I (Figure 1, top) and II (Figure 1, bottom). The AOT patterns are similar in most regions for the two products. Both products show elevated AOT levels in the  $30^\circ\text{N}$ – $45^\circ\text{N}$  latitude belts, off the west coast of Africa around  $5^\circ\text{N}$  (extending over the northern shores of Brazil), over the Bay of Bengal, and the South and East China Sea. However, significant differences are also evident in some regions, particularly in the middle and high latitudes of both hemispheres.

[16] The ASP patterns are less consistent than those for AOT, especially where AOT differences are significant. For example, product I indicates larger particles (smaller  $\alpha$ ) around  $45^\circ\text{S}$  and smaller particles (larger  $\alpha$ ) between  $15^\circ\text{S}$  and  $30^\circ\text{S}$ . The relatively small particles over the Atlantic between Africa and North America and between  $15^\circ\text{N}$  and  $30^\circ\text{N}$  suggested by product I are absent in product II. Detailed analyses are necessary to explain the similarities and the differences of the two aerosol products. To facilitate the analysis of the effects of cloud contamination and surface roughness, three CERES parameters, the Clear Strong Index (CSI), Cloud Fraction (CF), and Surface Wind Speed (SWS)

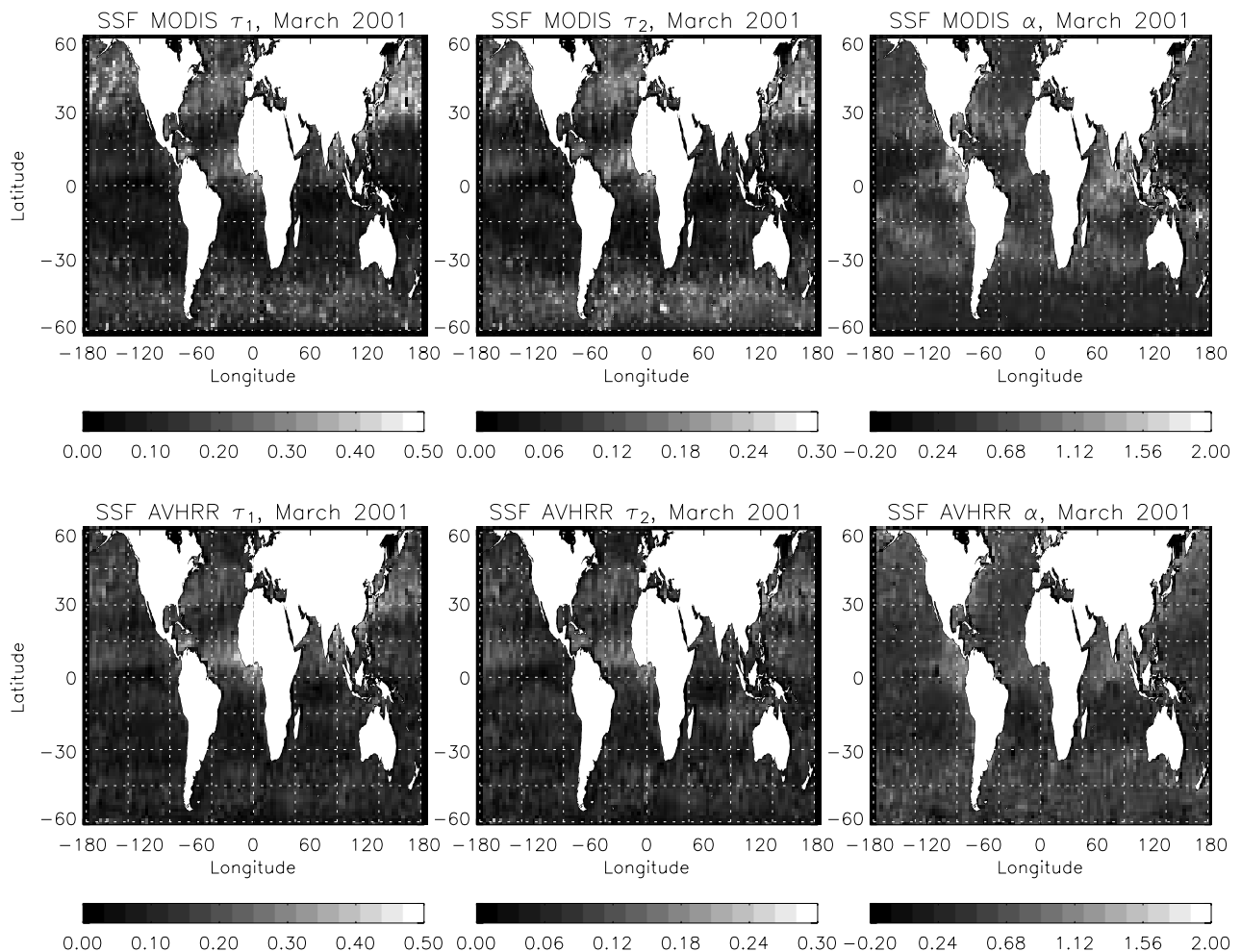


**Figure 1.** Monthly mean global maps ( $1^\circ \times 1^\circ$ ) of  $\tau_1$ ,  $\tau_2$ , and  $\alpha$  from SSFs for March 2001. (top) MODIS and (bottom) AVHRR-type retrievals. See color version of this figure at back of this issue.

are computed as described in Appendix B. CSI and CF are used to describe the extent of the clear-sky and cloudy condition within a CERES footprint and the SWS provides a measure of surface roughness. Since the results using CSI and CF are very similar so that only the results using CSI are presented below. The CSI is an objective evaluator of the absence of clouds in pixels used to retrieve the aerosol properties in the CERES data. Use of this discriminator could systematically eliminate scenes with very heavy dust concentrations that can be misclassified as clouds or weak clear scenes in the CERES mask (see Appendix B).

### 3.1. Optical Thicknesses

[17] Figure 2 displays the time series of global oceanic monthly mean values of  $\tau_1$  and  $\tau_2$  during 2001. Four different subsets of the data are considered. Scenario 1 uses all of the data and scenario 2 uses only strong clear conditions (with minimal cloud effect) defined by sampling the CERES footprints with CSI > 90%. Scenario 3 selects the smoothest surface by sampling the CERES footprints with SWS < 1 m/s and scenario 4 uses only the clearest and smoothest conditions defined by sampling the CERES footprints with both CSI > 90% and SWS < 1 m/s. On average,  $\tau(\text{MODIS})$  exceeds  $\tau(\text{AVHRR})$  year-round by  $\sim 0.02$  when

all of the matched SSF data are considered. This difference (solid minus dashed lines with the same symbol) is markedly reduced for the other three scenarios with  $\tau(\text{AVHRR})$  becoming slightly larger than  $\tau(\text{MODIS})$ . This result implies there are differences either in the cloud screenings, the response of the two aerosol retrievals to the cloud effect in the cloudy environment, or both. For example, during July  $\tau_1(\text{MODIS})$  rebounds after a June minimum for scenario 1 while  $\tau_1(\text{AVHRR})$  continues decreasing. For the other three scenarios,  $\tau_1$  for both methods increases from June to July. Thus differences in cases that appear cloudier in the CSI drive this marked discrepancy in July. The origin is not known at this time, but it could be a result of missing heavy dust scenes. These could be due to more frequent misclassifications of dusts as clouds by the CERES algorithm compared to the MODIS algorithm, but this cannot be confirmed without an in depth analysis of both methods' ability to separate dust and clouds. The remaining difference in scenario 4 is associated with the difference in the aerosol model and surface assumptions and the retrieval procedures in the two algorithms since the other effects have been minimized through the specified samplings.

[18] It should be pointed out the discrepancies between the AOTs for the smoothest surface and the clearest skies do

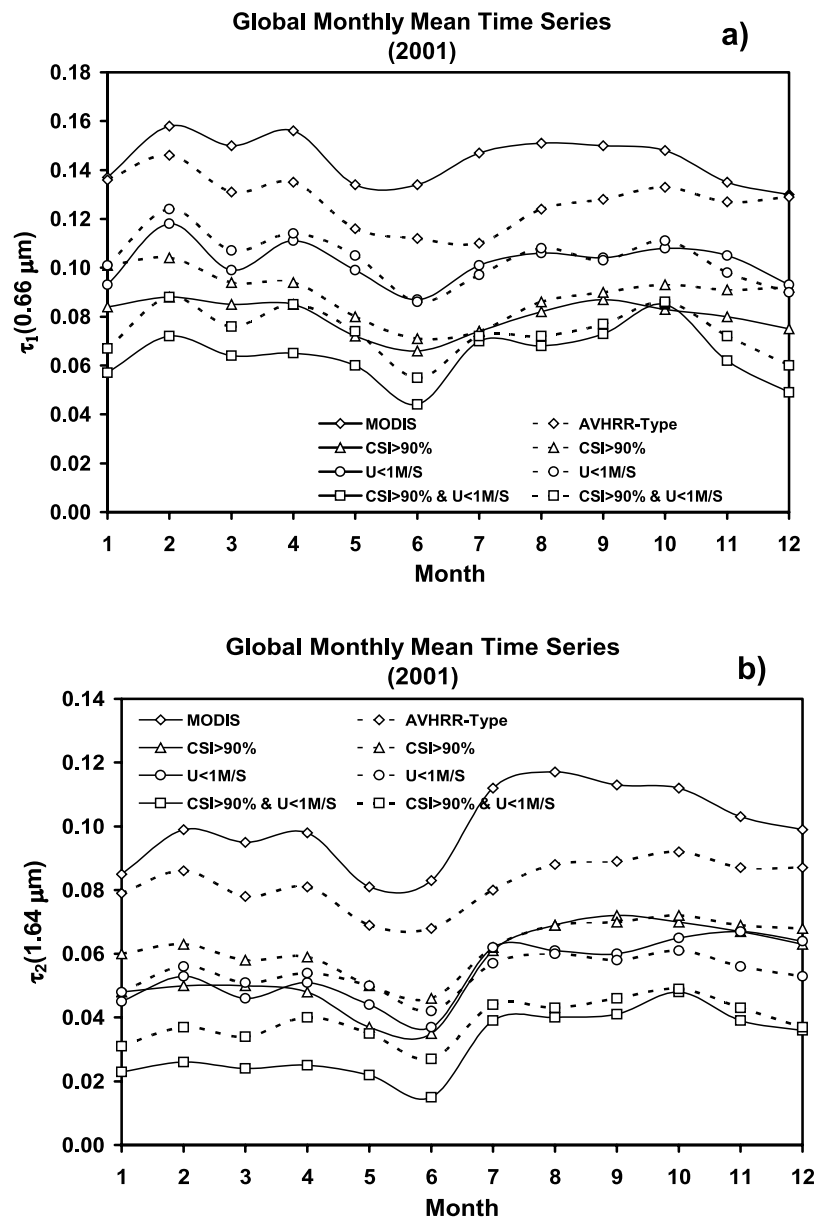


**Figure 2.** Time series of global monthly mean values of (a)  $\tau_1$  and (b)  $\tau_2$  during 2001. All or original data (diamonds), CSI > 90% (triangles), SWS < 1m/s (circles), and CSI > 90% and SWS < 1m/s (squares). MODIS values are in solid lines, and AVHRR-type values are in dashed lines.

not represent the global mean difference anymore because of the resulting limited sample size. However, it does indicate that the assumptions used by the two algorithms can make a significant difference in the regions covered by these limited sample points.

[19] The time series in Figure 2 show a change in the relative values of channels 1 and 2 AOTs for both products. Except for scenario 4, the  $\tau_1$  values are generally larger before than after June, while the trend is reversed for  $\tau_2$ . This pattern and the dips in June are thought to be an artifact caused by a change in the calibration uncertainties. According to the MODIS Characterization Support Team (MCST) report (available at [http://www.mcst.sai.biz/mcstweb/performance/terra\\_instrument.html](http://www.mcst.sai.biz/mcstweb/performance/terra_instrument.html)), the MODIS instrument experienced a Power Supply 2 (electronics Side-B) shut-

down anomaly and did not take science data during the time period from 15 June to 2 July of 2001. When the MODIS recovered, it was commanded to take science mode data using Power Supply 1 (or electronic Side-A). Different calibrations were applied to the reflected solar bands in the preanomaly and postanomaly stages and the calibration correction is relatively difficult to ascertain for the time period close to the power switch (J. Sun and X. Xiong, personal communication, 2004). Aerosol properties, especially size related parameters, are known to be very sensitive indicators of sensor radiometric uncertainties [Ignatov *et al.*, 1998] and the change in the  $\tau$  pattern observed in Figure 2 is most likely due to the power supply anomaly.

[20] To confirm this conclusion, the time series of aerosol fine mode fraction (a size parameter) from the standard

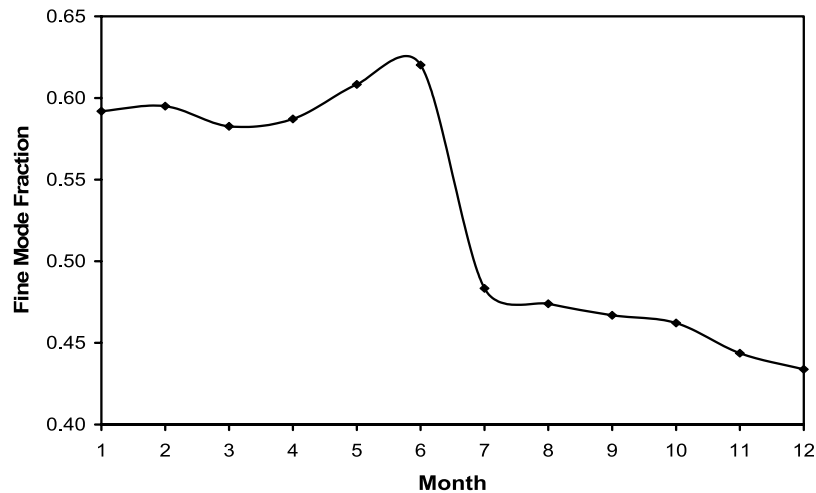


**Figure 3.** Time series of global monthly means of fine mode fraction of the MODIS aerosol during 2001. Data are taken from the standard MODIS aerosol product.

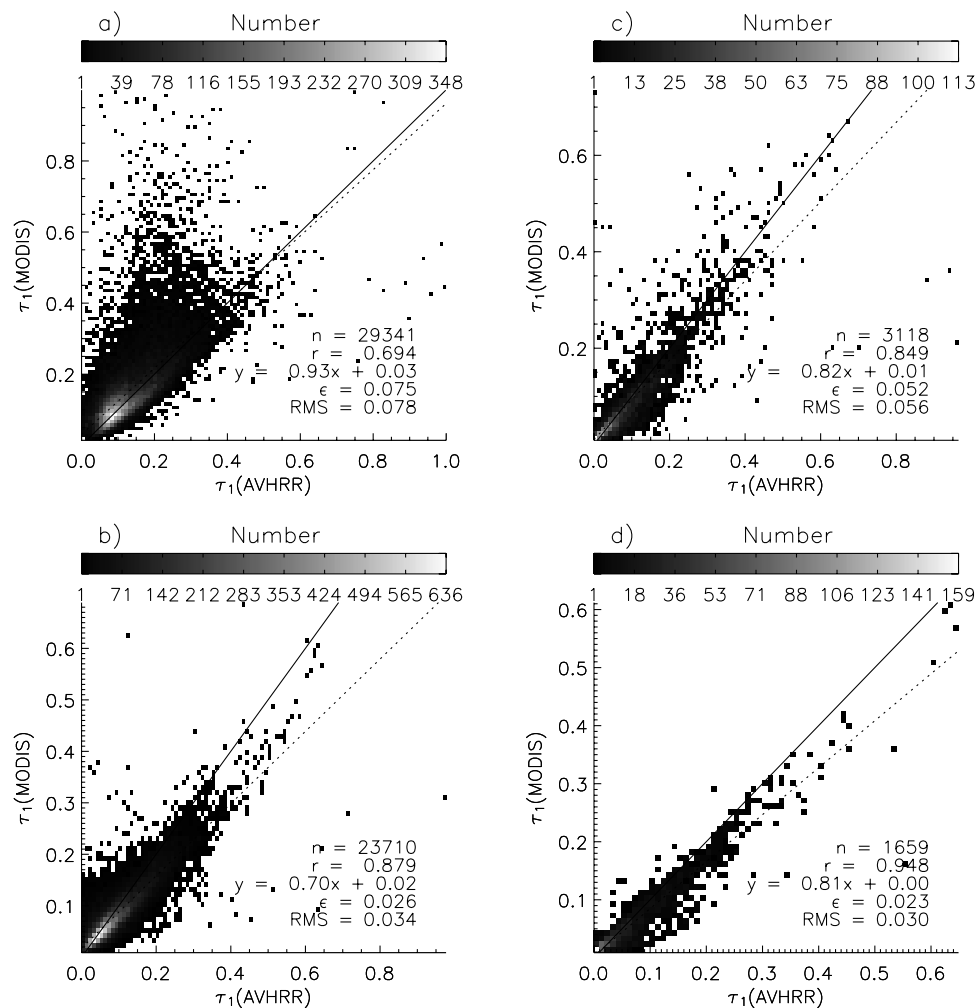


**Figure 4.** Scatterplots of  $\tau_1$  (at  $\lambda = 0.63 \mu\text{m}$ ) for the two SSF aerosol products during April 2001 for four subsets of the matched SSF data: (a) original data, (b) CSI > 90%, (c) SWS < 1m/s, and (d) CSI > 90% and SWS < 1m/s. Number density of the points is represented by the brightness. Solid line is the 1:1 relationship, and dashed line is a linear fit;  $n$  is the total number of points,  $r$  is correlation coefficient,  $\epsilon$  is standard deviation, and RMS is the root mean square error of the linear fit.

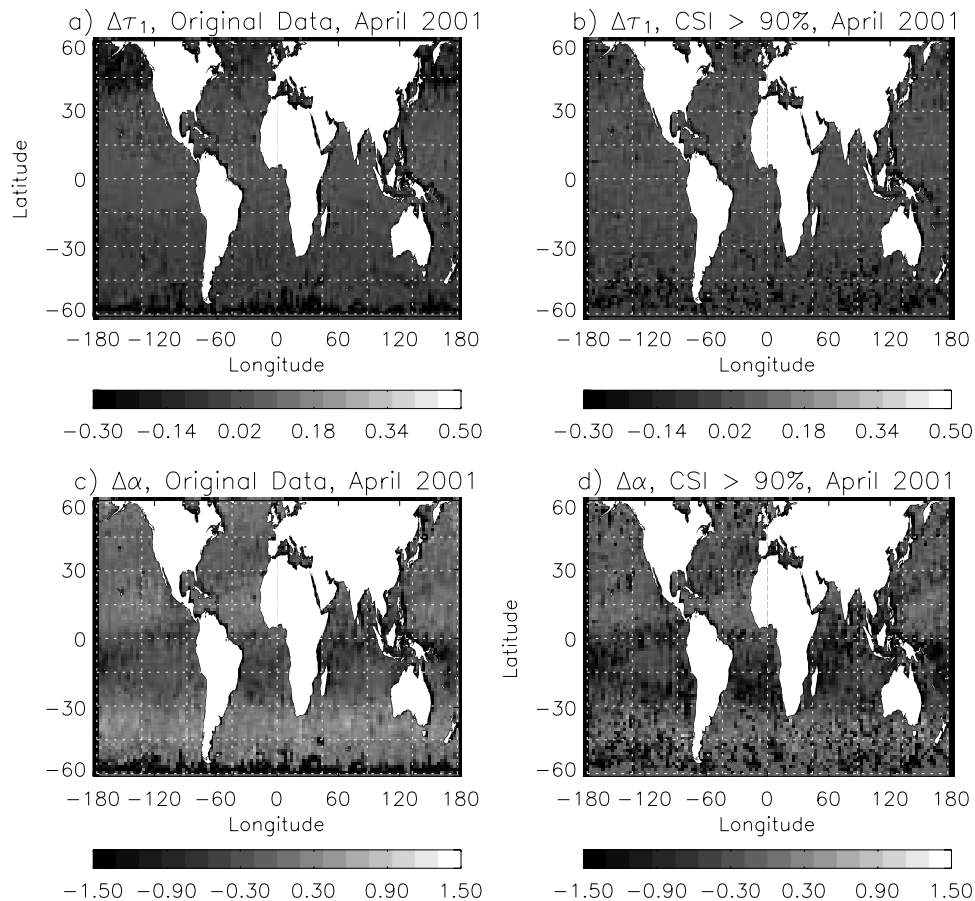


**Figure 5.** Global maps of monthly mean differences (AVHRR – MODIS) of (a and b)  $\tau_1$  and (c and d)  $\alpha$  for April 2001. Figures 5a and 5c show original data, and Figures 5b and 5d show CSI > 90%. See color version of this figure at back of this issue.

MODIS aerosol products is plotted in Figure 3. The fractional values change dramatically after the power supply anomaly. There is no natural explanation for this precipitous change after June except for the disruption associated with the power supply anomaly. More discussion of this issue is given by *Chu et al.* [2005]. In contrast, there are no similar changes in  $\tau$  and  $\alpha$  being observed for the same time period in the independent GACP AVHRR aerosol retrievals [see *Geogdzhayev et al.*, 2004, Figure 4]. The anomaly impact on AOT in Figure 2 is more evident for the three subset scenarios, especially in the 1.60- $\mu\text{m}$  channel. This is because the magnitudes of the aerosol signals contained in the solar reflectances for the three resampled scenarios are relatively small (especially in a longer-wavelength channel), resulting in a greater sensitivity to radiometric changes.

[21] The two data sets were also compared in scatterplots using the monthly mean  $1^\circ \times 1^\circ$  values derived from the original SSF footprints. Figure 4a shows an example for  $\tau_1$  during April. For the majority of the grids (with bright color), the two values of  $\tau_1$  compare reasonably well. Most of the outliers MODIS values are significantly larger than the AVHRR-type values. These outliers are responsible for many of the regional differences seen in Figure 1.

[22] To examine the causes of the outliers, the SSF footprints were resampled using same criteria employed for scenarios 2–4 to derive new monthly mean  $1^\circ \times 1^\circ$  values for the three conditions. The scatterplots of  $\tau_1$  for the

three conditions during April are displayed in Figures 4b–4d, respectively. For the strong clear condition (Figure 4b), the outliers disappeared almost completely (the RMS error decreased and the correlation increased). Figures 5a and 5b further display the April mean global maps of the  $\tau_1$  difference (AVHRR – MODIS) for scenarios 1 and 2. The large differences between the two methods, observed in the original data in the middle and high latitudes of both hemispheres are significantly reduced in the strong clear conditions, which is consistent with the scatterplot comparison. The annual mean global MODIS values of  $\tau_1$ ,  $\tau_2$ , and  $\alpha$  for 2001 are given in Table 1 along with their absolute and relative differences with the corresponding AVHRR-type values for the original and strong clear SSF data. The global mean differences in  $\tau$  ( $\Delta\tau$ ) and  $\alpha$  ( $\Delta\alpha$ ) between the two SSF aerosol products are less than 0.02. However,  $\Delta\tau$  is reduced to less than 0.01 when the cloud effects are minimized, but the value of  $\Delta\alpha$  increases to 0.13. These results further indicate there is a difference in the response of the two retrieval methods to the cloud effects, which may include both subpixel cloud contamination and real cloud effect on the surrounding aerosols.

[23] For the scenario 3 (Figure 4c), most of the outliers disappear (RMS decreases and correlation increases). However, only about 2 to 4 thousand grids over the globe are included in this least rough surface condition. For the clearest and smoothest conditions (Figure 4d), more outliers

**Table 1.** Annual Global Mean MODIS  $\tau_1$  and  $\tau_2$  and  $\alpha$  in the 2001 SSF Data<sup>a</sup>

	Original Data	Strong Clear (CSI > 90%)
$\tau_1$ (MODIS)	0.144	0.080
$\Delta\tau_1$ (AVHRR-MODIS)	-0.017	0.009
$\Delta\tau_1/\tau_1$ , %	-11.8	11.3
$\tau_2$ (MODIS)	0.100	0.056
$\Delta\tau_2$ (AVHRR-MODIS)	-0.018	0.006
$\Delta\tau_2/\tau_2$ , %	-18.0	10.7
$\alpha$ (MODIS)	0.419	0.493
$\Delta\alpha$ (AVHRR-MODIS)	0.019	-0.129
$\Delta\alpha/\alpha$ , %	4.5	-26.2

<sup>a</sup>Absolute and relative differences from the corresponding AVHRR-type values are also shown.

are removed compared to scenarios 2 and 3 (RMS and correlation are further improved), but even fewer grids included for these ideal conditions. Since the contributions from the other potential error sources have been minimized and the errors introduced by incorrect surface assumptions affect the offset more than the slope for a linear regression [Zhao *et al.*, 2002, 2003], the remaining difference between the two AOTs in Figure 4d are mainly due to the different assumptions of the aerosol model in the two algorithms. For  $\tau_1 < 0.15$ , the two values are close to each other. The difference increases with increasing  $\tau_1$  with the  $\tau$ (AVHRR) somewhat larger than  $\tau$ (MODIS). The MODIS retrieval uses several aerosol models to capture the variations in aerosol type over the globe that are missed with the fixed AVHRR model. The resultant differences in the AOTs are likely to be more prominent when  $\tau_1$  is large, which is consistent with the current results. Similar results were also obtained for January, July, and October and their regression statistics are summarized in Table 2.

[24] Figure 6 displays the zonal mean values of  $\tau_1$  and  $\alpha$  for both products for the original data and scenario 2 using the 4 sample months (January, April, July, and October). Most major zonal extremes (such as peaks at 50°S and 15°N, minimum at 20°S, etc) in  $\tau$  are similar for the two retrievals. The major differences in the AOT in the original data are poleward of 40° latitude, where the MODIS values are much larger than their AVHRR-type counterparts. The maximum  $\Delta\tau_1$  is greater than 0.1 around 50°N. These differences are reduced significantly for the strong clear condition mainly because of the reduction in the MODIS values. This suggests that the MODIS retrievals are subject to more cloud effects than the AVHRR-type retrieval, especially at high latitudes. The cloud effects here may include different responses in the retrieval algorithms to aerosols near the clouds or due to residual cloud contamination or both, which will be further investigated in section 4. Over the tropical oceans,  $\tau$ (AVHRR) is only slightly larger than ( $\Delta\tau_1 < 0.03$ )  $\tau$ (MODIS) for both scenarios. In general, the two AOT retrievals agree very well when the cloud effects are minimized. Because the potential for obtaining a CSI > 90 is greatly reduced for very heavy aerosol, primarily dust, loading (see Appendix B), this agreement may not hold for areas where heavy dust occurs.

### 3.2. Size Parameter

[25] Scatterplots of  $\alpha$  from the two methods were developed for the same four scenarios. Only the results for April

are shown in Figure 7 since the results for the other months are similar. For the unconditional matching (Figure 7a), the values of  $\alpha$  do not agree as well as those for  $\tau$ , probably because  $\alpha$  is more sensitive than  $\tau$  to the retrieval uncertainties, especially those associated with aerosol model assumptions [Ignatov *et al.*, 1998; Zhao *et al.*, 2002] as discussed earlier. The degradation in the RMS and correlation coefficients (Figures 7a–7d), quantifies the diminishing agreement between the two size parameters with improving retrieval conditions, a trend opposite to that seen for AOT in Figure 4. This variation suggests that cloud and surface roughness effects may mask differences in  $\alpha$  caused by the different aerosol model assumptions in the two methods. The differences in the two ASPs become more obvious after the most significant external effects have been minimized. In general,  $\alpha$ (MODIS) is larger than  $\alpha$ (AVHRR). Because several aerosol models are used in the MODIS retrieval, the dynamical range of  $\alpha$ (MODIS) also exceeds that of  $\alpha$ (AVHRR). Figures 5c and 5d also display the April mean global map of the difference,  $\alpha$ (AVHRR) –  $\alpha$ (MODIS). The differences are more obvious for strong clear conditions, which is consistent with the scatterplot comparison.

[26] The zonal means of  $\alpha$  in Figure 6 reveal that, for the original data,  $\alpha$ (MODIS) exceeds  $\alpha$ (AVHRR) by up to 0.2 in the tropics but falls below  $\alpha$ (AVHRR) at the highest latitudes. The differences at high latitudes drop significantly in strong clear conditions, indicating that these differences are associated with different responses of the two retrievals to cloud effects. However, the differences over the tropics are enhanced in the strong clear condition both in magnitude ( $\Delta\alpha$  can be up to  $\sim 0.3$ ) and in spatial coverage over the subtropics. This result suggests that the differences in the size parameters at low latitudes are caused by the aerosol model assumptions in the two

**Table 2.** Linear Regression ( $\tau_M = a + b\tau_A$ ) Statistics for  $\tau_1$ (MODIS) Versus  $\tau_1$ (AVHRR) for Selected Months During 2001<sup>a</sup>

Case	a	b	r	$\epsilon$	RMS
<i>January</i>					
1	0.02	0.90	0.749	0.048	0.049
2	0.00	0.81	0.895	0.023	0.030
3	0.00	0.84	0.891	0.038	0.043
4	0.00	0.83	0.927	0.019	0.025
<i>April</i>					
1	0.03	0.93	0.694	0.075	0.078
2	0.02	0.70	0.879	0.026	0.034
3	0.01	0.82	0.849	0.052	0.056
4	0.00	0.81	0.948	0.023	0.030
<i>July</i>					
1	0.04	0.88	0.726	0.065	0.071
2	0.03	0.60	0.808	0.025	0.034
3	0.02	0.78	0.816	0.054	0.058
4	0.02	0.64	0.854	0.032	0.043
<i>October</i>					
1	0.05	0.74	0.538	0.071	0.074
2	0.02	0.70	0.742	0.034	0.040
3	0.01	0.77	0.820	0.046	0.051
4	0.01	0.72	0.892	0.026	0.036

<sup>a</sup>Definitions are as follows:  $r$  is correlation coefficient,  $\epsilon$  is standard deviation, and the RMS is the root mean square error of the linear fit. The original SSF data, the strong clear, the smoothest surface, and the clearest and smoothest cases are indicated as cases 1, 2, 3, and 4, respectively.

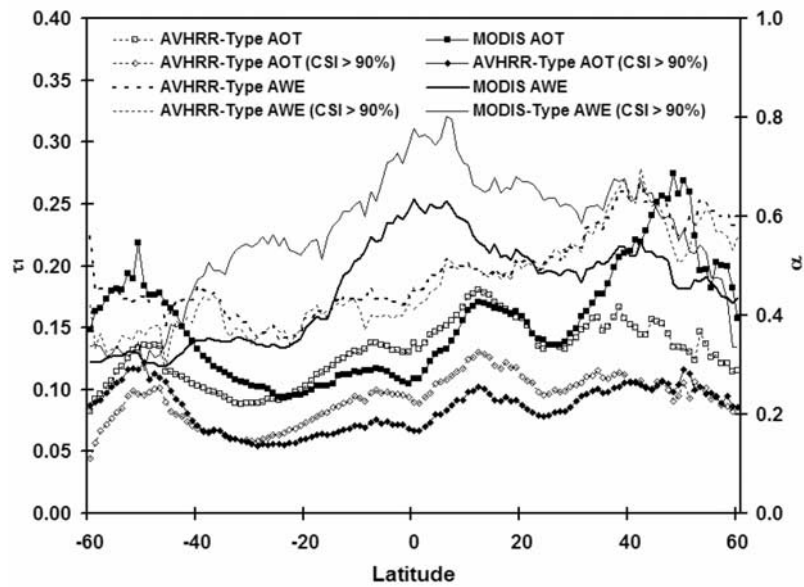


**Figure 6.** Zonal mean  $\tau_1$  and  $\alpha$  for the SSF MODIS and AVHRR-type aerosol products for the average of January, April, July, and October, 2001 for original SSF data and for CSI > 90%. AWE is Angström wavelength exponent  $\alpha$ .

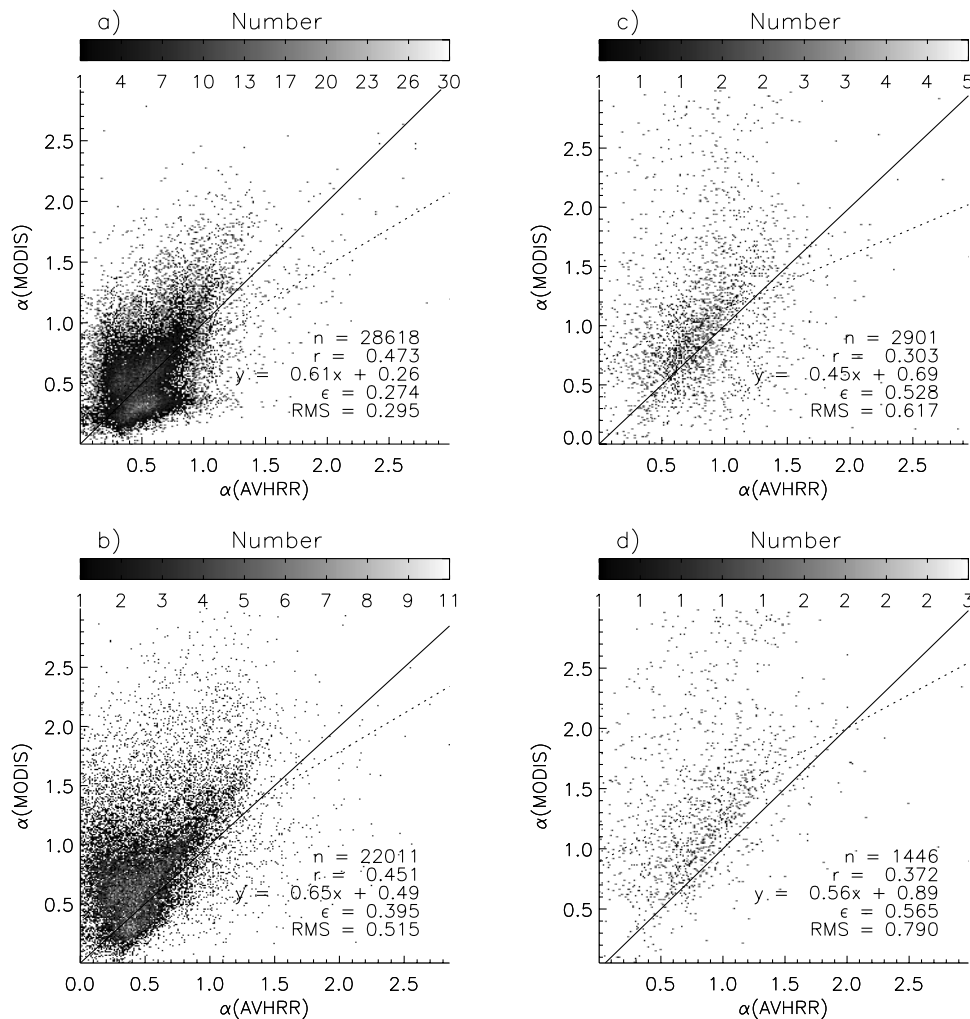


**Figure 7.** (a–d) Same as Figure 4 but for the size parameter  $\alpha$ .

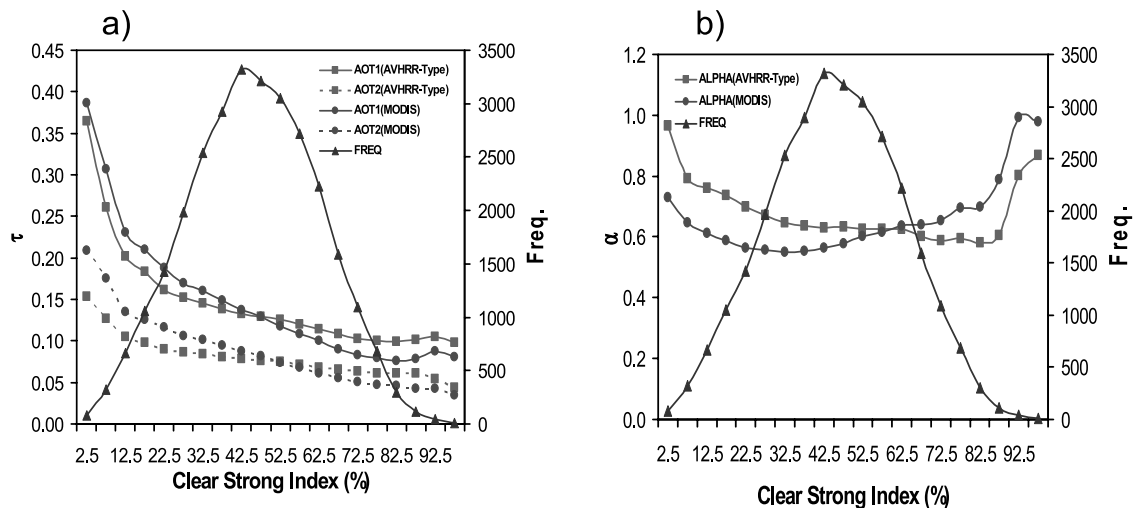


**Figure 8.** Globally averaged (a)  $\tau_1$  and  $\tau_2$  and (b)  $\alpha$  as functions of CSI for January 2001. The corresponding number (frequency) of footprints used for averaging in each CSI bin is also shown.

retrieval algorithms and not by cloud effects. The better agreement in  $\alpha$  at high latitudes for the strong clear cases suggests that cloud effects, not the aerosol models, are the primary source of the differences. Section 4 explores these differences in more detail.

#### 4. Effects of Cloud and Surface Roughness

[27] Subpixel cloud contamination or extra illumination of aerosols by sunlight from the sides of clouds may contribute to the cloud effect for satellite aerosol retrievals [Wagner *et al.*, 1997]. On the other hand, not all cloud effects are contamination. Aerosol optical thickness can increase in proximity to clouds because of the growth of particles with increasing relative humidity [e.g., Nemesure *et al.*, 1995]. Because of MODIS' high spatial resolution, aerosol retrievals can be performed closer to clouds and the enhanced aerosols in proximity to clouds can be detected. Similarly, surface roughness may not only affect the aerosol retrievals but also may be physically linked to an enhancement of aerosols through the injections from bubble bursts and the evaporation of sea spray [e.g., Heintzenberg *et al.*, 2000; Lewis and Schwartz, 2001]. The following analyses attempt to isolate the effects of clouds and surface roughness on the two aerosol products.

##### 4.1. Cloud Effect

[28] Figure 8 displays  $\tau_1$ ,  $\tau_2$ , and  $\alpha$  as functions of CSI for the two aerosol products in January. The values were averaged for the globe according to selected bins of CSI. The corresponding number (frequency) of footprints used for averaging in each bin is also plotted. CSI shows a strong negative correlation with  $\tau$  for both aerosol products (Figure 8a), especially when  $\text{CSI} < 20\%$ . CSI is positively correlated with  $\alpha$  for  $\text{CSI} > 85\%$  and negatively correlated for  $\text{CSI} < 20\%$  (Figure 8b).

[29] The dependence of AOT on CSI may be due to false aerosol signals associated with the subpixel cloud contamination and the extra illumination of aerosols by sunlight from the sides of clouds or due to a real aerosol signal that

either is enhanced in the moist environment around the clouds or due to the inability of the CERES cloud mask to render a “strong clear” classification in heavy aerosol conditions. Or, both enhanced aerosol signals and cloud effects are occurring simultaneously. Separating the false and real aerosol signals near the clouds is almost impossible using only the current satellite observations, especially for global monthly mean data. A definitive conclusion about the cloud effects on the satellite aerosol retrievals would require a combination of existing satellite observations (such as MODIS and MISR) with those from future space-based observing systems (such as CALIPSO and CloudSat) in addition to surface-based measurements of both aerosols and clouds.

[30] On the other hand, correlation analyses based on some statistical characteristics associated with the false and real aerosol signals near the clouds can be performed by using the multiple cloud, aerosol, and meteorological parameters that are available in the SSF data. Such analyses should provide additional insight into the issue of cloud effects on satellite aerosol retrievals. In general, cloud contamination should reduce the spectral dependence of the AOT derived from AVHRR [see Mischenko *et al.*, 1999], which results in smaller  $\alpha$  values that should change drastically from a noncontaminated regime to a contaminated regime. The sudden drop in  $\alpha$  in Figure 8b from strong clear ( $\text{CSI} > 90\%$ ) to clear ( $\text{CSI} < 90\%$ ) fits the cloud contamination characteristics so that the corresponding minor increase in AOT is likely to be associated with the false aerosol signal from cloud contamination. This analysis is also consistent with the ensemble AERONET validation presented by Zhao *et al.* [2005].

[31] However, the rapid increase (observed in Figure 8a) of  $\tau$  along with the corresponding slow increase of  $\alpha$  (see Figure 8b) in weak clear conditions ( $\text{CSI} < 20\%$ ) is not consistent with the cloud contamination characteristics. Thus the candidate that is responsible for the increase of  $\tau$  in the weak clear conditions is either a real aerosol signal or the surface roughness effect coexisting with the clouds that are often associated with a weather system. Surface rough-

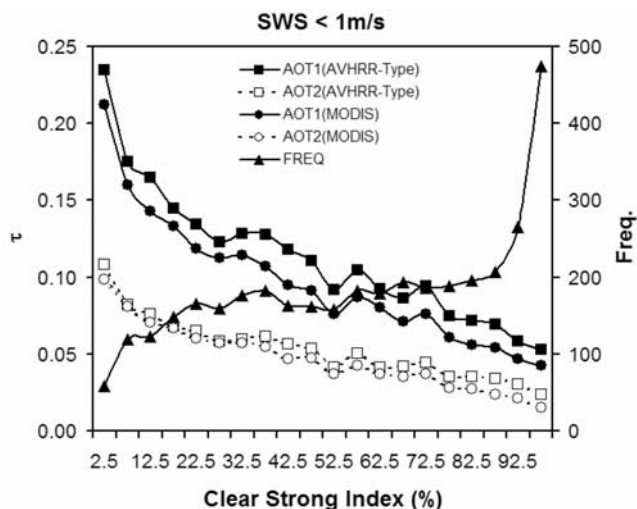


**Figure 9.** Same as Figure 8a except for pixels with SWS < 1 m/s.

ness is unlikely to be important because the increase of  $\tau$  for CSI < 20% remains even for the smoothest surface as defined with SWS < 1 m/s (Figure 9).

[32] The remaining candidates are that AOT is actually enhanced in the vicinity of clouds or that the CERES mask is frequently unable to classify scenes with heavy dust as strong clear scenes. Clouds can act as sources of new aerosol particles through in-cloud aqueous production and near-cloud particle nucleation [Hegg, 2001]. In addition, higher humidities in cloud fields can enhance the water vapor uptake by aerosol particles and the aerosol extinction even without generating new particles [Nemesure et al., 1995]. The cloud haloes [see Lu et al., 2002] often noticed also indicate that the aerosols are enhanced in the moist environment around the clouds. The correlations of  $\tau$  and  $\alpha$  with CSI observed here for CSI < 20% indicate the cloud effect on aerosol is significant even on a global scale.

[33] The increase of  $\tau$ (MODIS) with decreasing CSI is somewhat faster than that of  $\tau$ (AVHRR) in Figure 8a. It

may be associated with the fact that the MODIS cloud masking allows MODIS retrievals about 25% closer to cloudy pixels than the CERES cloud mask used in the AVHRR-type retrieval. The difference in the sensitivity of the two retrievals (due to different aerosol model assumptions) to the changes of aerosol properties from clear to weak clear conditions may also contribute to the slope discrepancy. For example, the MODIS retrieval may retrieve AOTs for pixels with heavy dust that were classified as cloudy by the CERES mask. More investigation beyond the scope of this paper is needed to examine each of these issues to understand the differences in the relationship between CSI and AOT.

**4.2. Surface Roughness Effect**

[34] The aerosol parameters were also correlated with surface wind speed (SWS). The January results in Figure 10 are typical in that  $\tau$  and  $\alpha$  smoothly increase and decrease with SWS, respectively. A secondary peak in  $\tau$  also appears at SWS = 2.5 m/s in Figure 10a. These variations of  $\tau$  and  $\alpha$  with changing SWS are maintained for the strong clear condition (CSI > 90%) as shown in Figure 11, except for loss of the secondary maximum in  $\tau$ .

[35] Since the surface wind speed is fixed for the MODIS (6 m/s) and AVHRR-type (1 m/s) retrievals, the surface reflectance is underestimated (or overestimated) for SWS greater (or less) than the assumed values. Correspondingly,  $\tau$  will be overestimated (or underestimated). The wind speed used in the MODIS retrieval is close to the global mean value, which is intentionally used to capture the global mean surface roughness for the MODIS aerosol retrieval. The wind speed of the AVHRR-type retrieval is biased low and will result in an overestimation of the retrieved global mean AOT with all other effects being equal. To reduce this overestimation, a fixed small diffusive reflection is added to the AVHRR-type retrieval. The MODIS algorithm assumes a dark surface, except at 0.55  $\mu$ m. The diffusive reflection is added for the AVHRR-type retrieval to best represent the global mean surface condition. Thus the difference between the computed surface reflectance for the global mean condition in the two aerosol retrievals is minor. The difference in AOTs between the two

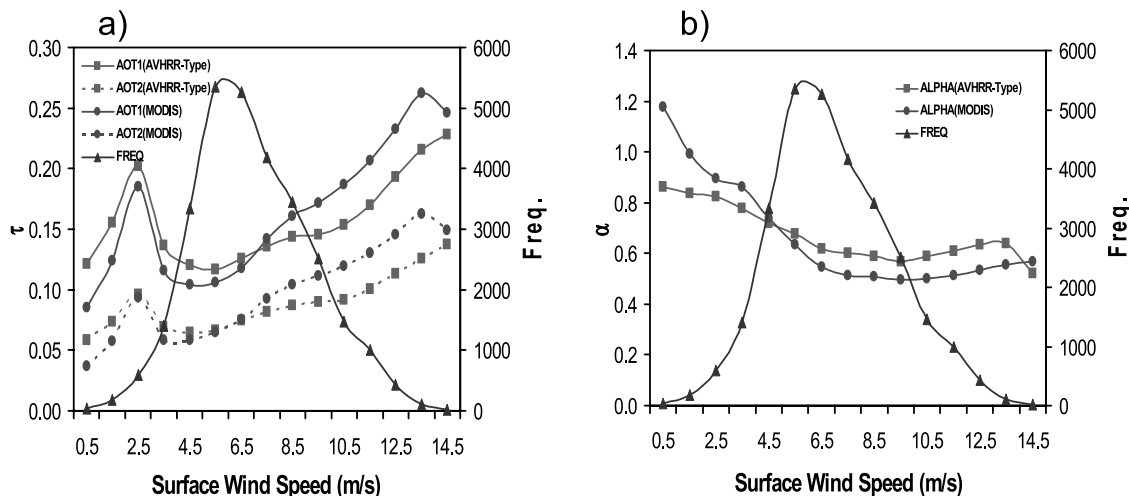


**Figure 10.** (a and b) Same as Figure 8 except as functions of SWS.

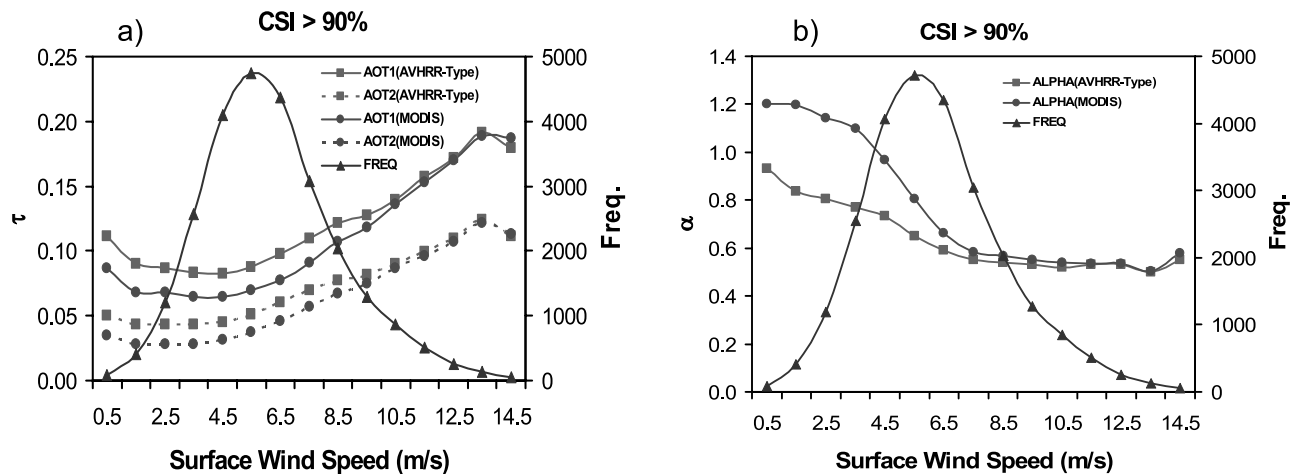


**Figure 11.** (a and b) Same as Figure 10 but for the strong clear case (CSI > 90%).

methods is not expected to be very large as seen in Figure 11 where  $\tau$ (AVHRR) is only slightly larger than  $\tau$ (MODIS).

[36] If surface roughness contamination is the only effect on the two SSF aerosol products, the two algorithms should agree best at the global mean surface wind (SWS  $\sim$  6 m/s) condition. This is not the case as observed in Figure 11a. There are at least two factors that may contribute to the observed dependence of  $\tau$  and  $\alpha$  on SWS. One is the presence of real aerosol signals associated with wind driven aerosols resulting from injection of bubble bursts and evaporation of sea spray over the rough ocean surface. Large particles with smaller  $\alpha$  values are mainly produced in this case. The other source is due to the cloud effect since large surface wind speed is often associated with a strong weather system and cloudy conditions as seen in Figure 12.

[37] Fortunately, the cloud effect can be separated from the wind driven aerosol signal by resampling the SSF footprints for the strong clear condition with a criterion of CSI > 90%. As a result, the cloud effect will be removed or minimized in the resampled data, which are displayed in Figure 11. Apparently, the secondary peak in Figure 10a that disappears in Figure 11a is due to the cloud effect. The general trends in  $\tau$  and  $\alpha$  seen in Figure 10 are maintained in Figure 11, which is consistent with the dependence of these parameters on SWS from the AERONET observations [see *Smirnov et al.*, 2003]. Near-surface observations also show that the sea spray generation of sea salt increases with SWS and become saturated at large wind speeds [e.g., *Heintzenberg et al.*, 2000; *Lewis and Schwartz*, 2001; *Andreas*, 1998]. Thus the aerosol optical properties derived from the two SSF aerosol retrievals should be similar at large wind speeds when the wind driven aerosols become dominant. This expected convergence of  $\tau$  and  $\alpha$  for the two SSF aerosol products occurs at SWS values around 10 m/s in Figure 11. All these characteristics suggest that the trend in the two aerosol products with the surface wind speed is mainly due to the wind driven aerosols and is not a retrieval artifact.

## 5. Summary and Conclusions

[38] As the first step in building connection and consistency between the advanced multichannel MODIS aerosol

retrieval and the simple two-channel AVHRR aerosol retrieval, a global comparison over ocean was performed using one year of Terra/CERES-MODIS SSF data. The comparisons indicate that the AOTs from the two SSF aerosol products are in reasonably good agreement, especially for small optical thicknesses. The difference increases with increasing AOT. Regional differences in the two optical thicknesses are mainly associated with the effects of clouds and surface roughness. The cloud effects are seen in both aerosol retrievals and are most obvious over high latitudes. The agreement between the size parameter  $\alpha$  of the two SSF aerosol products is not as close as that for optical thickness. Cloud effects and surface roughness reduce the AOT agreement but mask the difference in size parameter caused by differences in the aerosol model assumptions used by the two retrieval algorithms. An increase in AOT was found to increase with surface wind speed presumably because of an injection of wind driven aerosols. Cloud contamination appears to occur simultaneously with a real enhanced aerosol signal enhanced near clouds when subpixel cloud cover exceeds 20% in a SSF footprint. The cloud effects can have a noticeable global

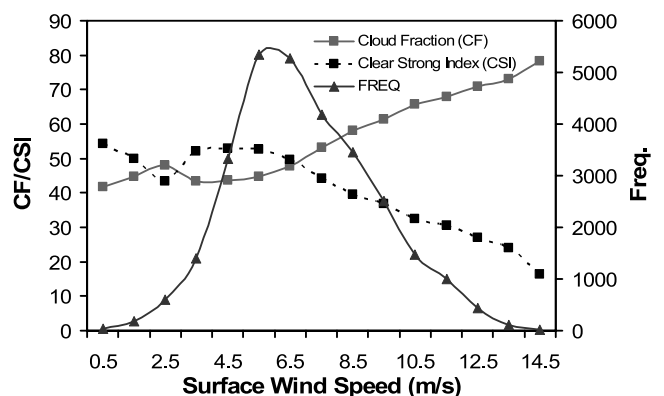


**Figure 12.** Global mean SSF Cloud Fraction (CF) and Clear Strong Index (CSI) as functions of Surface Wind Speed (SWS) for January 2001. The corresponding number (frequency) of the footprints used for averaging in each bin is also shown.

impact on the retrieved aerosol optical properties as shown in Table 1.

[39] Separating the cloud contamination effect from the enhanced aerosol loading near clouds is difficult without careful determination of cloud cover at relatively high (1 km) spatial resolutions at multiple wavelengths from well-calibrated data. The availability of both CERES and MODIS aerosol retrievals from well-calibrated global MODIS data has greatly facilitated the examination of the impact of clouds on aerosols. The enhanced cloud effect, not just cloud contamination, on aerosol properties deserves further study. Conclusive resolution of the issue will require a combination of existing satellite observations (such as MODIS and MISR) with those from active sensors on future space platforms, such as CALIPSO and CloudSat, and at the surface. In the meantime, the correlation analyses performed here can be considered as an initial effort to study the issue. The second paper [Zhao *et al.*, 2005] will demonstrate that the correlation analysis is more effective for the analysis of cloud and surface roughness effects on the aerosol retrievals at the regional scale since the problem can be more easily defined regionally compared to globally.

[40] From the results of this study it is concluded that, overall, the gain in aerosol retrieval accuracy over the ocean from the MODIS multichannel algorithm relative to the AVHRR two-channel algorithm is mostly in the improvement of aerosol size parameters rather than in optical thickness in a global mean sense, except for heavy aerosol loadings, which require additional analysis. Aerosol model assumptions are more important for regional retrievals, which will be further demonstrated in the regional evaluation of the two SSF aerosol products in part 2 of this study [Zhao *et al.*, 2005]. Cloud and surface roughness effects on the two SSF aerosol products require further investigation.

## Appendix A: Mapping Strategy of Two SSF Aerosol Products

[41] Both the standard MODIS (MOD04) aerosol granules ( $\sim 10$  km at nadir) and the resampled 1-km MODIS reflectances for the AVHRR type retrieval are mapped and averaged to the CERES field of view (FOV) with a resolution of about 20 km at nadir. The averaging is weighted with the CERES Point Spread Function (PSF) for each footprint to form two CERES SSF aerosol products (I and II). Only CERES footprints with at least one MODIS pixel (which satisfies the AVHRR-type retrieval criteria) are retained in the aerosol processing and those without MODIS pixels are discarded. Additionally, if a MODIS pixel falls outside all CERES FOVs, it is excluded from averaging computation in the mapping process. Thus overlaps of some CERES FOVs may occur and some MODIS pixels may be counted more than once in the averaging computation. For a CERES footprint containing at least one MODIS pixel, the MOD04 aerosol products in that footprint are averaged to form the CERES SSF aerosol product I. The AVHRR-type aerosol retrieval based on the “aerosol reflectance” for the same footprint serves as the CERES SSF aerosol product II.

[42] The MODIS pixel count statistics ( $N$ ) in a CERES footprint are stored as a SSF parameter, which is defined by the relative sizes of the CERES footprints and the MODIS pixels ( $N \cong [\text{CERES footprint size}/\text{MODIS pixel size}]^2$ ). If

both sensors point at nadir,  $N$  is  $\sim (20 \text{ km}/1 \text{ km})^2$  or  $\sim 400$ , and it changes with the CERES and the MODIS view zenith angles ( $\theta_C$  and  $\theta_M$ ). MODIS scans within  $\sim \pm 55^\circ$  off nadir in a fixed azimuth plane (FAP) perpendicular to the orbit plane (termed as cross-track scan), which provides a swath width of  $\sim 2330$  km from its altitude of 705 km. CERES allows scans up to  $\sim \pm 89^\circ$  off nadir in both FAP mode and rotated azimuth plane (RAP) mode and the corresponding SSF products are called flight model 1 (FM1) and flight model 2 (FM2) products, respectively. In the FAP mode, the CERES sensor can scan both cross-track (CT) and along-track (AT). For a FAP/CT scan, MODIS and CERES basically view the same scene when their view zenith angles are sufficiently close ( $\theta_C \approx \theta_M$ ). CERES footprints in the SSF data are confined by the maximum MODIS view zenith angle ( $\theta_M \sim \pm 55^\circ$ ) so that the maximum size of CERES footprint in the SSF data is about 50 km for the FAP/CT mode even though the footprint size of CERES at  $\pm 89^\circ$  view zenith angle can be quite large.

[43] In the SSF processing, only near-nadir MODIS pixels are retained for the FAP/AT scan. As a result, large SSF footprint size exists only in the RAP mode. Selecting two 1-week Terra SSF FM1 data in a FAP/CT mode and FM2 data in either a RAP or a FAP/AT mode, Ignatov *et al.* [2005] estimated the footprint size of the SSF data is between  $\sim 20$  and 50 km for FM1 and between  $\sim 20$  and 360 km for FM2. They also studied the accuracy of geographical referencing of the aerosol product in the above SSF mapping process considering the average footprint size for selected FM1 data is expected to be smaller than for selected FM2 data. They found the effect is only noticeable for large footprints in the SSF data when the CERES instrument is in RAP mode. The effect of geographical referencing will be smoothed by temporal and spatial averaging. In this regard, we prefer to use gridded and monthly mean values of the SSF aerosol data in our analysis.

## Appendix B: Complementary SSF Parameters

[44] Direct broadband measurements from the CERES instrument and products derived from these measurements are highly accurate because of the onboard calibration sources and the use of the latest anisotropic correction models in the CERES data processing [Loeb *et al.*, 2003]. MODIS provides accurate retrievals of cloud and aerosol properties since the retrieval algorithms are based on the combination of multiple spectral radiances with high spatial resolution and accurate onboard calibration. The CERES SSF data sets combine CERES radiation measurements, MODIS microphysical retrievals, and ancillary meteorology fields and form a comprehensive, high-quality compilation of satellite-derived cloud, aerosol, and Earth radiation budget information for radiation and climate studies. There are about 140 parameters in the SSF data [Geier *et al.*, 2003] and some of the nonaerosol parameters can be very useful for studying cloud and surface roughness effects on the two SSF aerosol products. The current analysis uses three of these SSF parameters: Clear Strong Index (CSI), Cloud Fraction (CF), and Surface Wind Speed (SWS). These three parameters are briefly described below.

[45] The CERES cloud mask scheme [Trepte *et al.*, 1999; Minnis *et al.*, 1999, 2002] involves a three-step analysis of each resampled MODIS pixel. The first step is a simple infrared test that flags pixels that are too cold to correspond to a surface and must be a cloud. The second step involves three kinds of threshold tests comparing pixel radiances to estimated background or clear-sky values for reflectance, infrared brightness temperature, and infrared/near-infrared brightness temperature difference, respectively. The threshold values are specified as functions of geographical location, time, and illumination-observation geometry, based upon empirical analyses, radiative transfer computations, and interpolations. If the three kinds of tests unanimously determine the pixel to be clear, this pixel is labeled “strong” clear. If one or two tests fail, a series of relaxed tests are performed to determine whether or not the pixel can be labeled as “weak” clear or cloudy. The third step, used for aerosol retrievals only, consists of homogeneity and adjacency tests that are based on the experience of the operational AVHRR aerosol retrieval [Stowe *et al.*, 1999; Vemury *et al.*, 2001]. The tests are used to eliminate residual cloud contamination and cloud shadow effect and are critical for aerosol retrievals. The spatial homogeneity test, which applies to a  $2 \times 2$  (or  $4 \text{ km} \times 4 \text{ km}$ ) clear-pixel array, requires that the difference between the maximum and minimum  $0.66\text{-}\mu\text{m}$  reflectances in a  $2 \times 2$  array is less than 0.003. The adjacency test further requires that all eight pixels surrounding the test pixel must be clear.

[46] The CERES cloud mask classifies each CERES subpixel (or resampled MODIS pixel) as clear, cloudy, bad data, or no retrieval. Each clear pixel is further categorized as “weak” or “strong” to indicate the degree of confidence in the selection (see the above discussions). A Clear Strong Index (CSI) is reported for each CERES footprint as one of the CERES parameters which is calculated as the PSF-weighted percent (from 0 to 100) of clear-strong pixels in the CERES field of view (FOV) relative to all the clear and cloudy pixels (bad data and no retrieval pixels are not included in the computation). If there are no clear-strong pixels in the FOV, the coverage is set to zero ( $\text{CSI} = 0$ ). If there are clear-strong pixels in the FOV, the coverage is set to 1% or greater ( $1 \leq \text{CSI} \leq 100$ ). It should be noted that the CERES cloud mask often misclassifies cloud-free pixels with heavy dust loadings ( $\tau_1 > 2$ ) as cloudy pixels so that those pixels will rarely accompany a strong clear classification.

[47] In addition to CSI, a Clear Area Percent Coverage (CAPC) is also reported in the SSF data. The CAPC is based on the subpixel cloud fraction and is also PSF weighted. The average is performed for all the clear and cloudy pixels without considering bad data and no retrieval pixels. It is set to zero when the percent coverage is less than 0.5%. A Cloud Fraction (CF) is derived in our analysis by subtracting the SSF CAPC from 100.

[48] The U and V components of surface wind speed are also reported in the SSF data. These two SSF parameters are taken from ECMWF and GMAO assimilation wind fields and linearly interpolated to the latitude and longitude of CERES footprints. A linear interpolation is also performed in the temporal domain to produce the hourly SSF values from the 6-hourly input data samples. Since sea surface conditions, such as roughness, foam, and whitecaps

are strongly related to the surface wind speed, the Surface Wind Speed (SWS) derived from the SSF U and V parameters is a good indicator of the variability of the surface condition and roughness. A more detailed description of the SSF parameters and their definition is given by Geier *et al.* [2003].

[49] **Acknowledgments.** We would like to acknowledge the DAAC of the NASA Langley for supplying the CERES/SSF data. We also appreciate the large effort of CERES and MODIS scientists in collecting, processing, and producing the data used in this study. Two anonymous reviewers’ constructive comments and suggestions on the manuscript are greatly appreciated. This work was supported by the NASA Radiation Program through grant RSP-0022-0005, the NPOESS Integrated Program Office (IPO) through the Risk Reduction Project at the NOAA/NESDIS, and the CERES Project. The views, opinions, and findings contained in this report are those of the authors and should not be construed as an official NOAA or U.S. Government position, policy, or decision.

## References

- Ackerman, S., K. Strabala, P. Menzel, R. Frey, C. Moeller, and L. Gumley (1998), Discriminating clear-sky from clouds with MODIS, *J. Geophys. Res.*, **103**, 32,141–32,157.
- Andreas, E. L. (1998), A new sea spray generation function for wind speeds up to 32 m/s, *J. Phys. Oceanogr.*, **28**, 2175–2184.
- Chu, D. A., Y. J. Kaufman, L. A. Remer, B. Schmid, J. Redemann, K. Knobelspiess, J.-D. Chern, J. Livingston, P. B. Russell, and W. Ridgway (2005), Evaluation of aerosol properties over ocean from Moderate Resolution Imaging Spectroradiometer (MODIS) during ACE-Asia, *J. Geophys. Res.*, **110**, D07308, doi:10.1029/2004JD005208.
- Geier, E. B., R. Green, D. P. Kratz, P. Minnis, W. F. Miller, S. K. Nolan, and C. B. Franklin (2003), *CERES Data Management System: Single Satellite Footprint TOA/Surface Fluxes and Clouds (SSF) Collection Document*, release 2, version 1, 212 pp., Radiat. and Aerosol Branch, Atmos. Sci. Res., NASA Langley Res. Cent., Hampton, Va. (Available online at [http://asd-www.larc.nasa.gov/ceres/collect\\_guide/SSF\\_CG.pdf](http://asd-www.larc.nasa.gov/ceres/collect_guide/SSF_CG.pdf)).
- Geogdzhayev, I. V., M. I. Mishchenko, L. Liu, and L. Remer (2004), Global two-channel AVHRR aerosol climatology: Effects of stratospheric aerosols and preliminary comparisons with MODIS and MISR retrievals, *J. Quant. Spectrosc. Radiat. Transfer*, **88**, 47–59.
- Hegg, A. (2001), The impact of clouds on aerosol population, *IGActivities*, **23**, April. (Available at <http://www.igac.noaa.gov/newsletter/igac23/hegg.html>)
- Heintzenberg, J., D. C. Covert, and R. Van Dingenen (2000), Size distribution and chemical composition of marine aerosols: A compilation and review, *Tellus, Ser. B*, **52**, 1104–1122.
- Higurashi, A., and T. Nakajima (1999), Development of a two channel aerosol retrieval algorithm on global scale using NOAA/AVHRR, *J. Atmos. Sci.*, **56**, 924–941.
- Ignatov, A., and L. L. Stowe (2000), Physical basis, premises, and self-consistency checks of aerosol retrievals from TRMM VIRS, *J. Appl. Meteorol.*, **39**, 2259–2277.
- Ignatov, A., and L. L. Stowe (2002), Aerosol retrievals from individual AVHRR channels, part I: Retrieval algorithm and transition from Dave to 6S radiative transfer model, *J. Atmos. Sci.*, **59**, 313–334.
- Ignatov, A., L. Stowe, and R. Singh (1998), Sensitivity study of the Angstrom exponent derived from AVHRR over oceans, *Adv. Space Res.*, **21**, 439–442.
- Ignatov, A., P. Minnis, N. Loeb, B. Wielicki, W. Miller, S. Sun-Mack, D. Tanre, L. Remer, I. Laszlo, and E. Geier (2005), Two MODIS aerosol products over ocean on the Terra and Aqua CERES SSF datasets, *J. Atmos. Sci.*, **62**, 1008–1031.
- Intergovernmental Panel on Climate Change (2001), *Climate Change 2001: The Scientific Basis*, 870 pp., Cambridge Univ. Press, New York.
- Kaufman, Y. J., et al. (1997), Remote sensing of tropospheric aerosol from EOS-MODIS over the land, *J. Geophys. Res.*, **102**, 17,051–17,067.
- Kaufman, Y. J., D. Tanre, and O. Boucher (2002), A satellite view of aerosols in the climate system, *Nature*, **419**, 215–223.
- King, M. D., Y. J. Kaufman, D. Tanre, and T. Nakajima (1999), Remote sensing of tropospheric aerosols: Past, present, and future, *Bull. Am. Meteorol. Soc.*, **80**, 2229–2259.
- Lewis, E. R., and S. E. Schwartz (2001), Size-dependent sea-salt aerosol production fluxes: A critical review, *Eos Trans. AGU*, **82(47)**, Fall Meeting Suppl., Abstract A21A-0057.
- Loeb, N. G., N. Manalo-Smith, S. Kato, W. F. Miller, S. Gupta, P. Minnis, and B. A. Wielicki (2003), Angular distribution models for top-of-atmosphere radiative flux estimation from the Clouds and the Earth’s Radiant

- Energy System instrument on the Tropical Rainfall Measuring Mission satellite. Part I: Methodology, *J. Appl. Meteorol.*, *42*, 1748–1769.
- Lu, M.-L., R. A. McClatchey, and J. H. Seinfeld (2002), Cloud halos: Numerical simulation of dynamical structure and radiative impact, *J. Appl. Meteorol.*, *41*, 832–848.
- Martins, J. V., D. Tanre, L. Remer, Y. Kaufman, S. Matto, and R. Levy (2002), MODIS cloud screening for remote sensing of aerosols over oceans using spatial variability, *Geophys. Res. Lett.*, *29*(12), 8009, doi:10.1029/2001GL013252.
- Minnis, P., D. P. Kratz, J. A. Coakley Jr., M. D. King, D. Garber, P. Heck, S. Mayor, D. F. Young, and R. Arduini (1995), Cloud optical property retrieval (subsystem 4.3), in *Clouds and the Earth's Radiant Energy System (CERES) Algorithm Theoretical Basis Document*, vol. III, *Cloud Analyses and Radiance Inversions (Subsystem 4)*, edited by CERES Science Team, *NASA RP 1376*, vol. 3, 135–176.
- Minnis, P., D. F. Young, B. A. Wielicki, P. Heck, X. Dong, L. Stowe, and R. Welch (1999), CERES cloud properties derived from multi-spectral VIRS data, paper presented at EOS/SPIE Symposium on Remote Sensing, Int. Soc. for Opt. Eng., Florence, Italy, 20–24 Sept.
- Minnis, P., D. F. Young, B. A. Wielicki, S. Sun-Mack, Q. Z. Trepte, Y. Chen, P. W. Heck, and X. Dong (2002), A global cloud database from VIRS and MODIS for CERES, paper presented at 3rd International Asia-Pacific Environmental Remote Sensing Symposium: Remote Sensing of Atmosphere, Ocean, Environment, and Space, Int. Soc. for Opt. Eng., Hangzhou, China, 23–27 Oct.
- Mischenko, M., I. V. Geogdzhayev, B. Cairns, W. B. Rossow, and A. Lacis (1999), Aerosol retrievals over the oceans by use of channels 1 and 2 AVHRR data: Sensitivity analysis and preliminary results, *Appl. Opt.*, *38*, 7325–7341.
- Mischenko, I. M., B. Cairns, J. E. Hansen, L. D. Travis, R. Burg, Y. J. Kaufman, J. Vanderlei Martins, and E. P. Shettle (2004), Monitoring of aerosol forcing of climate from space: Analysis of measurement requirements, *J. Quant. Spectrosc. Radiat. Transfer*, *88*, 149–161.
- Nemesure, S., R. Wagener, and S. E. Schwartz (1995), Direct shortwave forcing of climate by anthropogenic sulfate aerosol: Sensitivity to particle size, composition, and relative humidity, *J. Geophys. Res.*, *100*, 26,105–26,116.
- Penner, J. E., et al. (2002), A comparison of model- and satellite-derived optical depth and reflectivity, *J. Atmos. Sci.*, *59*, 441–460.
- Remer, L. A., et al. (2005), The MODIS aerosol algorithm, products and validation, *J. Atmos. Sci.*, *62*, 947–973.
- Smirnov, A., B. N. Holben, T. F. Eck, O. Dubovik, and I. Slutsker (2003), Effect of wind speed on columnar aerosol optical properties at Midway Island, *J. Geophys. Res.*, *108*(D24), 4802, doi:10.1029/2003JD003879.
- Stowe, L. L., A. M. Ignatov, and R. R. Sigh (1997), Development, validation, and potential enhancements to the second-generation operational aerosol product at the National Environmental Satellite, Data, and Information Service of the National Oceanic and Atmospheric Administration, *J. Geophys. Res.*, *102*, 16,923–16,932.
- Stowe, L. L., P. A. Davis, and E. P. McClain (1999), Scientific basis and initial evaluation of the CLAVR-1 global clear/cloud classification algorithm for the Advanced Very High Resolution Radiometer, *J. Atmos. Oceanic Technol.*, *16*, 656–681.
- Tanré, D., M. Herman, and Y. J. Kaufman (1996), Information on the aerosol size distribution contained in the solar reflected spectral radiances, *J. Geophys. Res.*, *101*, 19,043–19,060.
- Tanré, D., Y. J. Kaufman, M. Herman, and S. Matto (1997), Remote sensing of aerosol over oceans from EOS-MODIS, *J. Geophys. Res.*, *102*, 16,971–16,988.
- Trepte, Q., Y. Chen, S. Sun-Mack, P. Minnis, D. F. Young, B. A. Baum, and P. W. Heck (1999), Scene identification for the CERES cloud analysis subsystem, paper presented at AMS 10th Conference on Atmospheric Radiation, Am. Meteorol. Soc., Madison, Wis., 28 June to 2 July.
- Vemury, S., L. L. Stowe, and V. R. Anne (2001), AVHRR pixel level clear-sky classification using dynamic thresholds (CLAVR-3), *J. Atmos. Oceanic Technol.*, *18*, 169–186.
- Wagener, R., S. Nemesure, and S. E. Schwartz (1997), Aerosol optical depth over oceans: High space- and time-resolution retrieval and error budget from satellite radiometry, *J. Atmos. Oceanic Technol.*, *14*, 577–590.
- Wielicki, B. A., B. R. Barkstrom, E. F. Harrison, R. B. Lee III, G. L. Smith, and J. E. Cooper (1996), Clouds and the Earth's Radiant Energy System (CERES): An Earth observing system experiment, *Bull. Am. Meteorol. Soc.*, *77*, 853–868.
- Wielicki, B. A., R. N. Green, C. J. Tolson, and A. Fan (1997), *Clouds and the Earth's Radiant Energy System (CERES) Algorithm Theoretical Basis Document, Overview of Cloud Retrieval and Radiative Flux Inversion (Subsystem 4.0)*, release 2.2, 2 June.
- Zhao, X., L. Stowe, A. Smirnov, D. Crosby, J. Sapper, and C. R. McClain (2002), Development of a global validation package for satellite oceanic aerosol optical thickness retrieval based on AERONET observations and its application to NOAA/NESDIS operational aerosol retrievals, *J. Atmos. Sci.*, *59*, 294–312.
- Zhao, X., I. Laszlo, B. N. Holben, C. Pietras, and K. J. Voss (2003), Validation of two-channel VIRS retrievals of aerosol optical thickness over ocean and quantitative evaluation of the impact from potential sub-pixel cloud contamination and surface wind effect, *J. Geophys. Res.*, *108*(D3), 4106, doi:10.1029/2002JD002346.
- Zhao, X., O. Dubovik, A. Smirnov, B. N. Holben, J. Sapper, C. Pietras, K. J. Voss, and R. Frouin (2004), Regional evaluation of an advanced very high resolution radiometer (AVHRR) two-channel aerosol retrieval algorithm, *J. Geophys. Res.*, *109*, D02204, doi:10.1029/2003JD003817.
- Zhao, X., I. Laszlo, P. Minnis, and L. Remer (2005), Comparison and analysis of two aerosol retrievals over the ocean in the Terra/Clouds and the Earth's Radiant Energy System—Moderate Resolution Imaging Spectroradiometer single scanner footprint data: 2. Regional evaluation, *J. Geophys. Res.*, *110*, D21209, doi:10.1029/2005JD005852.

I. Laszlo and T. X.-P. Zhao, Office of Research and Application, NOAA National Environmental Satellite, Data, and Information Service, 5200 Auth Road, Camp Springs, MD 20746, USA. (xuepeng.zhao@noaa.gov)

P. Minnis, Atmospheric Sciences Division, NASA Langley Research Center, Hampton, VA 23681, USA.

L. Remer, Laboratory for Atmospheres, NASA Goddard Space Flight Center, Greenbelt, MD 20771, USA.

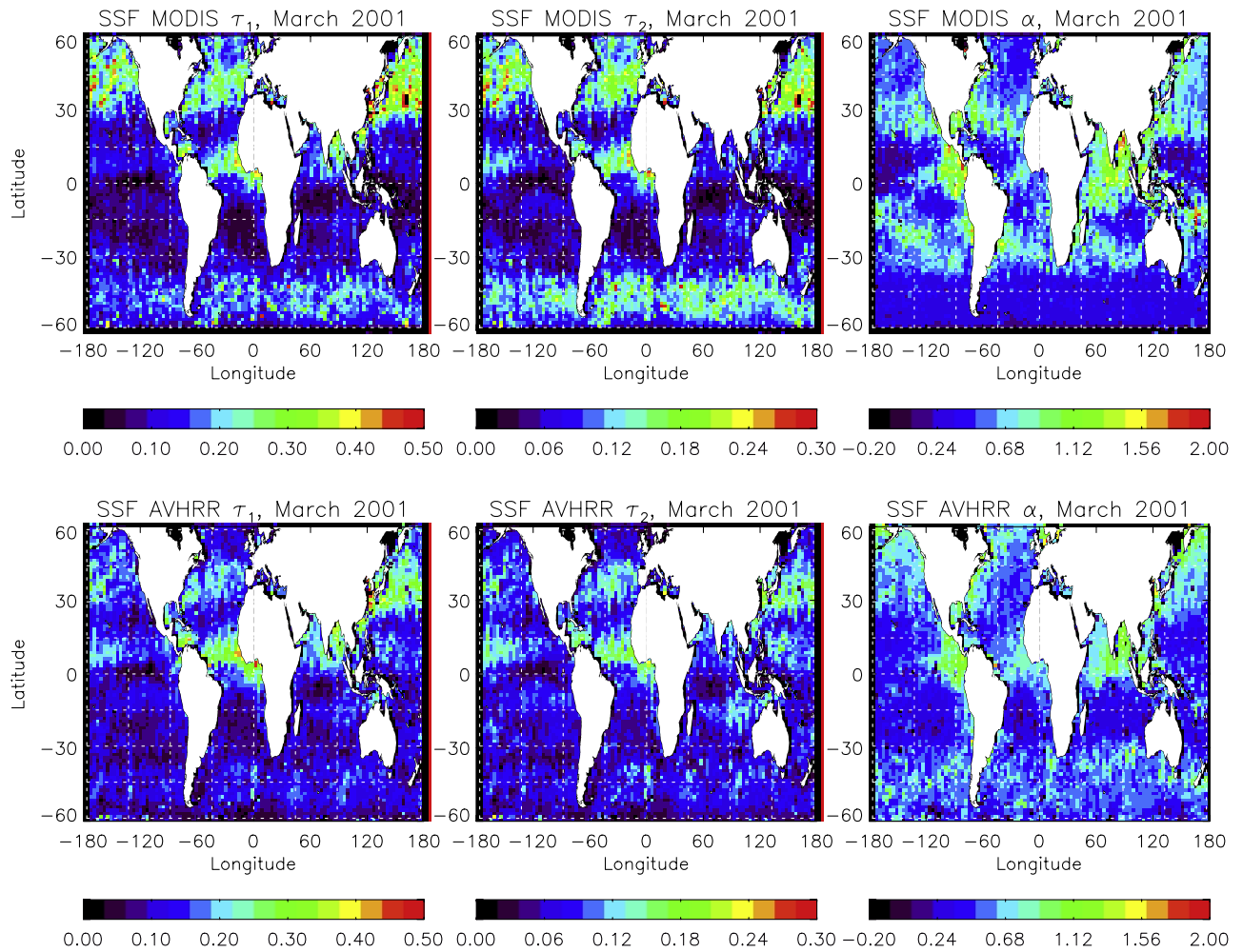


**Figure 1.** Monthly mean global maps ( $1^\circ \times 1^\circ$ ) of  $\tau_1$ ,  $\tau_2$ , and  $\alpha$  from SSFs for March 2001. (top) MODIS and (bottom) AVHRR-type retrievals.

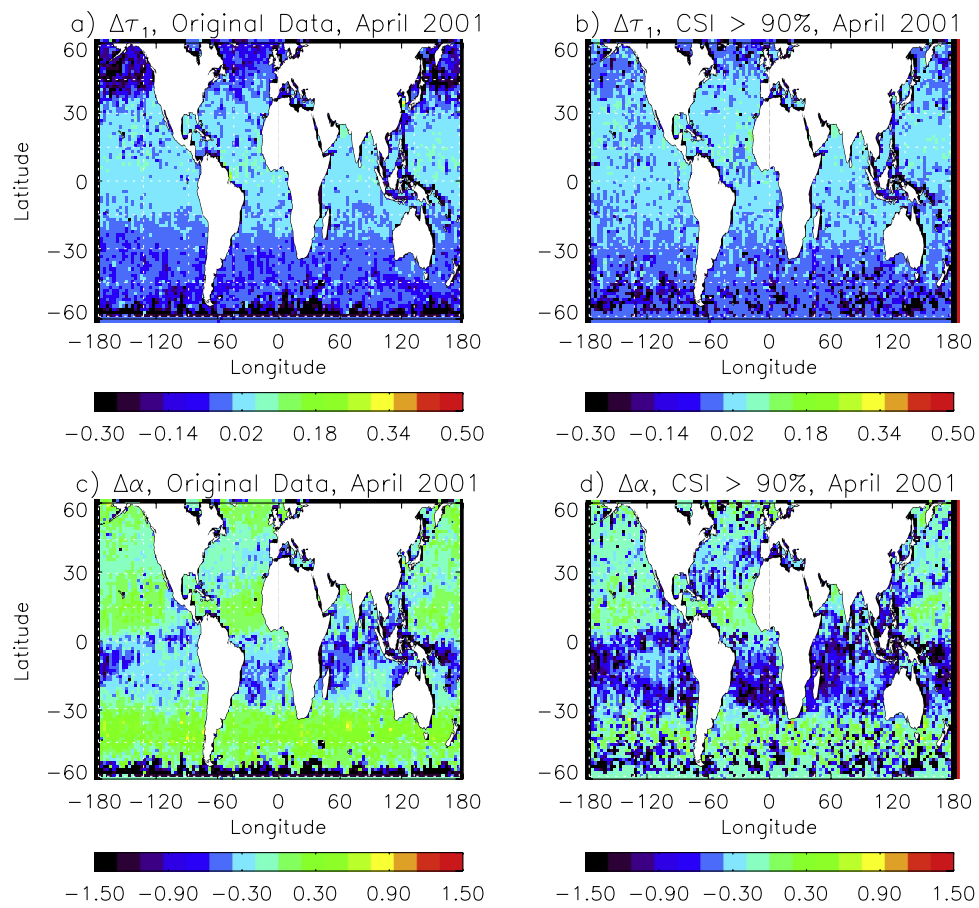


**Figure 5.** Global maps of monthly mean differences (AVHRR – MODIS) of (a and b)  $\tau_1$  and (c and d)  $\alpha$  for April 2001. Figures 5a and 5c show original data, and Figures 5b and 5d show CSI > 90%.